Validation of a field deployable reactor for in-situ formation of NOM-engineered nanoparticles corona

* Corresponding author

Authors: Narjes Tayyebi Sabet Khomami [a], Allan Philippe [a*], Abd Alaziz Abu Quba [a], Oliver J. Lechtenfeld [b,c], Jean-Michel Guigner [d], Stefan Heissler [e], Gabriele E. Schaumann [a]

[a] iES Landau, Institute for Environmental Sciences, Koblenz-Landau University, Fortstrasse 7, 76829 Landau, Germany. [b] UFZ - Helmholtz-Centre for Environmental Research, Department Analytical Chemistry, Research Group BioGeoOmics, 04318 Leipzig, Germany. [c] ProVIS – Centre for Chemical Microscopy, UFZ – Helmholtz-Centre for Environmental Research, 04318 Leipzig, Germany. [d] IMPMC, Sorbonne University, CNRS – UMR 7590, MNHN, Paris, France. [e] Institute of Functional Interfaces IFG, Karlsruhe Institute of Technology KIT, Hermann-von-Helmholtz-Platz 1, D-76344 Eggenstein-Leopoldshafen, Germany.

Abstract

Despite the numerous studies about the sorption of dissolved organic matter (DOM) onto nanoparticles, the extrapolation of laboratory-results to environmental conditions is currently impossible. Indeed, the complex dynamics of DOM under variable environmental conditions are not completely reproducible under control conditions. In this study, we propose a different approach by exploring a method for exposing nanoparticles to realistic environmental conditions in natural river water by using dialysis membranes as passive reactors. Inside this reactor, the complexity and the temporal variability of a large number of environmental parameters (DOM structure and composition, temperature, inorganic ions, pH, etc.) are reproduced, while colloidal and particulate interferences remain separated. To verify this assumption, we determined the concentration of the water components and nanoparticles (n-TiO_2, 20-50 nm) inside and outside the reactor before and after exposure to river water. In river water, more than 90% of the n-TiO_2 remained inside the reactor while DOM retained its molecular composition/characteristics after passing through the membrane (DOC, Fluorescence EEM, FT-ICR MS). For most elements and anions, the concentrations inside and outside the reactor did not differ indicating a good permeability for inorganic constituents (IC, ICP-OES); however, the concentrations of Al, Fe, Mn, and nitrate were lower. Membrane fouling, in terms of pore size distribution, was investigated using NMR relaxometry and AFM in fluid mode; no significant reduction in pore size was observed under the applied conditions during seven days of exposure. Finally, ATR-FTIR and CHNS analysis of n-TiO_2 before and after

exposure to the river water revealed that sorption of DOM occurred under field conditions. Therefore, we could demonstrate the validity and the potential of this method.

Keywords

Passive reactor, dialysis membrane, n-TiO_2, natural organic matter, NMR relaxometry, AFM, FT-ICR MS

Introduction

For the last 15 years, engineered nanomaterials (ENMs) have attracted growing academic and industrial interests with a wide range of applications in cosmetics, building materials, medicine, and energy storage. [1] Among these materials, titanium dioxide nanoparticles (n-TiO_2) represent the second most important part of ENMs production worldwide (550–5500 t/year) and is expected to increase in the near future. [2–4] This high production as well as diverse applications leads to inevitable emission of n-TiO_2 into the environment. These nanoparticles can enter aquatic systems either directly or indirectly via wastewater treatment plants or landfills. [5–7]

The fate and biological activity of n-TiO_2 in the aquatic systems depend not only on nanoparticle properties, but also on the characteristics of the receiving water environment including dissolved organic matter (DOM), multivalent cations and natural colloids. [8] DOM, mainly containing humic substances, polysaccharides, and proteins, represents one of the most dynamic fractions of organic matter in aquatic systems. Depending on the biochemical conditions and concentration in waters, they typically range from 0.1 to 10 mg/L. [9] Once n-TiO_2 are released into natural systems, interactions of NOM with these nanoparticles will affect their fate, transport, and risk assessments. [10] There are a multitude of studies to understand NOM sorption on titanium dioxide nanoparticles; [10–17] nonetheless, most of them have been conducted in the laboratory under highly simplified controlled conditions which do not consider, for instance, DOM dynamic structure dependency on water parameters affect the sorption mechanism. Therefore, the results are difficult or even impossible to extrapolate to natural conditions. Hence, there is still a lack of methods allowing a realistic exposure of nanoparticles to temporal environmental conditions including NOM composition, temperature, background electrolyte concentration, and pH for testing hypotheses developed from lab experiments.

Passive sampling is an environmental monitoring technique based on free flow of analyte molecules from the sampled medium to a collecting medium as a result of a difference in chemical potentials. [18–20] The device used for passive sampling is usually membrane dialysis. [20] Dialysis is a simple process in which small solutes diffuse from a high concentration solution to a low concentration solution across a semipermeable membrane. There are

several studies using dialysis membranes in passive sampling. Vroblesky *et al.* used regenerated cellulose dialysis samplers to measure the volatile organic compounds in different wells. [21] Vencalek *et al.* applied cellulose ester dialysis bags to separate Cu nanoparticles from the dissolved Cu species in freshwater mesocosms. [22] Benes *et al.* determined the state of trace elements in natural waters using cellulose membrane. [23]

In this study, we present the first steps of the evaluation of a realistic river water exposure method for n-TiO_2 inspired from the concept of passive sampling. n-TiO_2 nanoparticles were selected to test the method since they do not dissolve in water and the sorption of DOM components on these nanoparticles is well studied. [24,25] The proposed method relies on membrane dialysis, i.e. the dialysis bag considered as a passive reactor retaining n-TiO_2 nanoparticles inside while DOM can diffuse inside. Furthermore, the natural colloids cannot enter which simplifies the extraction of the nanoparticle after exposure. In order to apply this method to environmental waters, the membrane needs to meet several requirements:

- Retaining nanoparticles, permeable to non-colloidal water components (suitable molecular weight cut-off of the membrane).
- Robustness towards environmental variation (pH, temperature, water flow, aquatic organisms).
- The permeability of the membrane should remain constant during the exposure. Fouling is the principal mechanism affecting the permeability under environmental conditions. [26,27]

In order to assess these issues, we exposed the dialysis bags (for improved readability, we will refer to "dialysis bag" for denoting the passive reactor) in river water and determined the concentration of the main organic and inorganic components inside and outside. Furthermore, we investigated the pore structure before and after exposure using NMR relaxometry and AFM in fluid mode.

Finally, we carried out a field exposure of n-TiO_2 in a river and evaluated the sorption of DOM of the river water onto n-TiO_2 by characterizing nanoparticles before and after river exposure using ATR-FTIR and CHNS analyses. The results present the proof-of-concept of using dialysis bags and the validity of implementing this method to study the interactions of NOM and engineered nanoparticles under real environmental conditions.

Material and methods

Material

Biotech Cellulose ester (CE) Membranes with three different molecular weight cut off (20, 100, and 300 kDa) were purchased from Repligen (Formerly Spectrum). The specifications provided by the supplier can be found in **Table 1**. Before usage, the membranes were soaked first in 10% (v/v) ethanol-water for 10 minutes, rinsed with distilled water (DW) and soaked in DW for removing glycerin and achieve maximum membrane permeability. [28] The membranes were stored in DW until further usage. Pre-experiments with dialysis bags using clip type closure resulted in the loss of 50% of the deployed dialysis bags, damaged under the movement induced by the river flow (30-40 cm/s, OTT MF pro, Germany). Therefore, cylindrical dialysis bags with screw-on caps showing 100% resistance over one week were selected for this study (**Figure S1**). Aeroxide® n-TiO_2 P25 powder was purchased from Degussa, Germany.

Table 1 specifications of the dialysis bag

specifications	Membrane type	Physical Appearance	Packaging	pH limit	Temperature limit	Total Length	Membrane Diameter
	Float-A-Lyzer® Cellulose Ester (CE)	Opaque, Rigid	Dry with glycerine	2-9	4-37˚C	10 cm	10 mm

HR-TEM (n-TiO_2)

For nanoparticles characterization, 5 µL of 1 g/L n-TiO_2 suspension was placed on a TEM grid and dried at ambient conditions. Transmission Electron Microscopy (TEM) measurements were performed using a JEOL 2100F (JEOL Ltd., Tokyo, Japan), field emission gun instrument operating at 200 kV equipped with a polar piece ultra-high resolution. Images were recorded on an UltraScan 4000 Gatan (Gatan Inc., Pleasanton, CA, United States) camera with a 4k × 4k pixels CCD.

Sampling and characterization of the river water

The experiments were conducted with water collected from the River Queich (latitude: 49.205510, longitude: 8.088081) in Landau in der Pfalz, Germany in May-September 2018 (In case of a complementary experiment, the date is mentioned). For the sake of simplicity we will refer to “river water” for denoting the water sampled at this place. The characteristics of the river water were fairly stable over this period of time (**Table S1**).

Samples were collected in a polypropylene canister at 1 m from the river bank. The pH was measured on site (SG2-FK SevenGo, Mettler Toledo, Schwerzenbach, Switzerland). The samples were transported immediately to the nearly located laboratory, and were stored in the dark at 4° C. Multi-parameter analyser (Consort C863, Turnhout, Belgium) was used to measure electrical conductivity. Dissolved organic carbon (DOC) concentration was determined after filtration with 0.45 µm PTFE filters (Altmann, Germany) using a TOC analyzer (multi N/C 2100, Analytik Jena AG, Jena, Germany). The concentrations of Al, Ba, Ca, Cu, Fe, K, Mg, Mn, Na, Sr, and Zn the river water samples were measured using inductively coupled plasma optical emission spectroscopy (ICP-OES, 720, Agilent Technologies, Santa Clara, USA). Digestion procedure for determination was done similar to the literature with some modifications. [5] 10 mL of the river water was dried at 95 °C, cooled down at room temperature before adding 2.5 mL of hydrogen peroxide (30 %, Rotipuran®, Carl Roth, Germany). After 10 min standing at room temperature, 5 mL of sulfuric acid (95 %, Rotipuran®, Carl Roth, Germany) was added dropwise before being progressively heated until ebullition (225°C). After one hour at 225°C, the samples were cooled down at room temperature and diluted into a 100 mL volumetric flask prior to ICP-OES analysis. All samples were measured in triplicates. Ion chromatography (Professionel IC 881 Metrohm) was used to analyze anions. Dissolved oxygen was measured using PyroScience Optical Oxygen Sensor. The chemical and physical information of the river summarized in the supporting materials **Tables S1-3**.

Permeability of dialysis bags toward n-TiO_2

To check the permeability of dialysis bags for the nanoparticles used in this study, a 300 mg/L suspension of n-TiO_2 was prepared and sonicated (ultrasound bath) for 10 minutes. The dialysis bags were filled with 5 ml of n-TiO_2 suspension, and placed in a 50 ml polypropylene centrifuge tube filled with 35 ml river water. The tubes were shaken at 200 rpm using a horizontal shaker for a specified time. Samples were collected from outside of the dialysis bags, prior to Ti-content determination using ICP-OES. The samples were digested following Philippe et al. [5] The ICP-OES measurements were carried out for Ti at an emission wavelength of 334.941 nm. All samples were measured in triplicates.

Determination of the equilibrium time

The dialysis bags were filled with 5 ml distilled water, and placed into a 50 ml polypropylene centrifuge tube filled with 35 ml river water. The tubes were shaken at 200 rpm using a horizontal shaker at room temperature (21 ° C). After the specified time, samples were collected from inside and outside of the dialysis bags, filtered using 0.45 µm PTFE (Altmann, Germany), and analyzed for TOC.

NMR relaxometry

The transverse relaxation time (T_2) in ^{1}H NMR relaxometry measures the decay of magnetization of proton spins after excitation from their dephasing in time-dependent fluctuation of the magnetic field caused by adjacent nuclei (T_2). [29] Thus, T_2 distribution can be related to the pore size distribution with lower T_2 corresponding to water present in small pores while larger T_2 correspond to large pores as well as "free" bulk water. Cellulose compounds (dialysis bag) depict recognizable bimodal T_2 distribution, [30] which was also observed for the cellulose ester membrane of the dialysis bag and represent the hierarchical porous structure of the membrane. For measuring the spin-spin relaxation time (T_2) of dialysis bags in different media (distilled water, river water with and without n-TiO_2), the dialysis bags were completely emptied and measured immediately to avoid drying of the membrane. All samples were measured in triplicates. A Bruker Minispec MQ, Version 2.2 (Bruker, Karlsruhe, Germany) was used at a magnetic field strength of 0.176T (proton Larmor frequency of 7.5MHz); applying 64 scans, with the recycled delay of 10 s. The gain was adjusted for each sample individually such that 70–80% signal intensity was achieved. Calculations and figures were done using Matlab R2014 a, and Origin 7.5. [31]

AFM

The dialysis bags were cut to approximately 2 * 1 cm^2 pieces. They were fixed on a steel-disc using instant glue, and stored in distilled water, or river water until measurement. The atomic force microscopy (AFM, Dimension Icon, Bruker Corporation, USA) analyses were conducted using tapping mode in water media, with New Sharp Nitride Lever tips (SNL, Bruker, USA) with a radius of 2 nm (nominal value). Sample mounting for AFM fluid experiments along with the probe calibration procedures were performed as recommended in the Bruker protocols. [32,33] To measure the pore size of the dialysis bag, images were captured from six random locations and further processed for pore size estimation (ImageJ). The pores area was determined automatically after black/white picture conversion and contrast adjustment. The obtained areas were used to determine a hydrodynamic diameter for each pore (also known as pore thickness or opening diameter) defined as the diameter of the largest circle inscribed in a pore following the equation (1):

(1)

where A (area) equals the total number of pixels enclosed by the pore boundary, and P (perimeter) is the number of pixels on the boundary. The results of the six regions of interest were combined to have a set of representative data. Analysis of the images and corresponding calculations were carried out using the program ImageJ v1.52a. and Origin 7.5.

169 *Field exposure experiment*

170 To avoid the damage of dialysis bags by the stream flow of the river or the aquatic animals, each dialysis bag
171 was enclosed in a perforated polyethylene plastic canister (approximate perforation diameter: 0.3 mm). The
172 dialysis bags were filled by 5 ml distilled water (control), or a freshly prepared and sonicated (10 minutes in an
173 ultrasound bath) n-TiO_2 300 mg/L suspension (three replicates), and placed in the canister (**Figure S2**). The
174 canisters were fixed to an anchor and immersed in the river about 1 m from the river bank. After a week, the
175 content of the dialysis bags was collected in a 15 mL polypropylene centrifuge tube and immediately transferred
176 to the laboratory for further analyses. It is worth mentioning, the realistic concentration of n-TiO_2 in surface
177 waters is low (e.g. 0.55-16 µg/L). [34] However, the majority of current analytical techniques used for sorption
178 studies are not capable of working with concentrations in µg/L range; therefore, the applied n-TiO_2 concentration
179 (300 mg/L) was way too higher than the realistic ones. Nonetheless, in the field experiment, there is a large
180 excess of available DOM for nanoparticles; hence, high concentration of n-TiO_2 (300 mg/L) inside the bags is
181 not changing the ratio of sorbate/sorbent significantly.

182

183 *Fluorescence spectroscopy*

184 The collected river water samples were centrifuged (Universal 320, Hettisch, Bäch, Switzerland) at 4500 rpm
185 (3283 g) for 30 min. Since the n-TiO_2 nanoparticles were visibly agglomerated, this speed was sufficient to
186 collect them at the bottom and the supernatant was transparent under this condition. The supernatant was taken
187 for further measurements. Fluorescence Excitation/emission matrix (EEM) of the samples were recorded on a
188 PerkinElmer LS 55 Fluorescence spectrometer in the emission (Em) range of 200-700 nm by varying the
189 excitation (Ex) wavelength from 250 to 450 nm in 20 nm increments with a scan rate of 1200 nm/ min.
190 Excitation and emission slits were both 10 nm. Since a linear calibration curves (fluorescence intensity versus
191 fluorophore concentrations, $R^2 = 0.9991$) was obtained after serial dilutions of the river water, we considered the
192 filter effects as negligible for this river sample. No corrections for scattering effects were applied to the data as
193 there were no observable overlapping of the fluorescence and scattering peaks. The EEM spectra were plotted
194 using Origin 7.5.

195 *CHNS*

For each measurement of river water, 250 ml of the river water was filtered with 0.45 µm PTFE filters (Altmann, Germany), and freeze-dried (Christ, Osterode, Germany) for two continuous days at -40 °C and 0.12 mbar and two more days at -60 °C and 0.011 mbar. TiO_2 nanoparticles exposed to the river water were centrifuged at 4500 rpm (3283 g) for 30 min. The supernatant was withdrawn carefully to the last drop and the centrifugate was freeze dried as described above. For CHNS elemental analysis, 4-15 mg of samples were weighed into tin boats (LabNeed GmbH, Nidderau, Germany) together with around 20 mg of WO_3 powder (LabNeed GmbH, Nidderau, Germany), and measured using CHNS varioMicroCUBE (Elementar, Langenselbold, Germany). Sulfanilamide (Elementar GmbH, Langenselbold, Germany) was used as a reference sample. Computation of the Euclidian distances was carried out using the program R Studio (Version 1.0.143).

ATR-FTIR

The nanoparticle pellet collected after centrifugation and also the river water sample collected on the last day of field experiment were freeze-dried as for CHNS. For ATR-FTIR measurements, a Bruker Tensor 27 IR spectrometer (Bruker Optics, Ettlingen, Germany) with a Bruker Platinum ATR accessory, single reflectance diamond crystal, 45° angle of incidence, was used. Some milligrams of the samples were applied directly on the ATR-crystal. Spectra were measured against an air background. Each spectrum comprised 32 coadded scans with a spectral resolution of 4 cm^{-1} in the 3600−370 $cm^{-}1$ range. The absorption spectra were depicted using Origin 7.5 software.

FT-ICR-MS sample preparation and measurement

River water samples (5 mL) were extracted via solid-phase extraction using an automated sample preparation system (FreeStyle, LC Tech) on 50 mg styrene-divinyl-polymer type sorbens (Bond Elut PPL, Agilent Technologies) to desalt the sample for subsequent DI-ESI-MS according to Raeke et al. [35]. The SPE-DOM was eluted with 1 mL methanol (Biosolv), diluted to 20 ppm and mixed 1:1 (v/v) with ultrapure water immediately prior FT-ICR MS analysis. Carbon based extraction efficiency was approx. 50% (for river water). SRFA measured in triplicate was used to check instrument variability and solvent and extraction blanks were prepared.

An FT-ICR mass spectrometer equipped with a dynamically harmonized analyzer cell (solariX XR, Bruker Daltonics Inc., Billerica, MA) and a 12 T refrigerated actively shielded superconducting magnet (Bruker Biospin, Wissembourg, France) instrument was used in ESI negative ionization mode (capillary voltage: 4.3 kV). Extracts were analyzed in random order with an autosampler (infusion rate: 10 µL min-1). For each spectrum, 256 scans were co-added in the mass range 150 3000 m/z with 25 ms ion accumulation time and 4

MW time domain (resolution@400 m/z ca. 500 000). Mass spectra were internally linear calibrated with a list of peaks (250-600 m/z, n > 143) commonly present in terrestrial DOM and the mass accuracy after calibration was better than 0.13 ppm. Peaks were considered if the signal/noise (S/N) ratio was greater than four.

FT-ICR-MS data evaluation

Molecular formulas were assigned to peaks in the range 150-750 m/z allowing for elemental compositions C_{1-60} $^{13}C_{0-1}$ H_{1-122} O_{1-40} N_{0-2} S_{0-1} $^{34}S_{0-1}$ with an error range of ±0.5 ppm according to Lechtenfeld et al.[36] Briefly, the following rules were applied: $0.3 \leq H/C \leq 2.5$, $0 \leq O/C \leq 1.0$, $0 \leq N/C \leq 1.5$, $0 \leq DBE \leq 20$ (double bound equivalent, DBE = 1+1/2 (2C−H+N), Koch et al. [37]), $8 \leq DBE\text{-}O \leq 8$ (Herzsprung et al. [38,39]) , and element probability rules proposed by Kind and Fiehn [40]. Isotope formulas were used for quality control but removed from the final data set as they represent duplicate chemical information. All molecular formulas present in the medium blank or instrument blank samples were excluded from the peak lists. 4668 - 5022 formulas were assigned with no multiple assignments to 16568 - 17423 peaks above noise level). Molecular formulas and compounds are used synonymously throughout the text, although no molecular structures are known.

Relative peak intensities were calculated based on the summed intensities of all assigned monoisotopic peaks in each sample. Van Krevelen diagrams for river water samples inside and outside the dialysis bags were used to depict differences in relative intensities (ΔRI) for each individual molecular formula according to Equation 2. [41]

(2)

where *sample* refers to the water inside the bag (with n-TiO_2) and *reference* is the water outside the bag (river water). To test the effect of instrumental variability on the ΔRI values six SRFA samples (Suwannee River Fulvic Acid) were measured on the same day. Relative standard deviations (RSD) were calculated from the normalized intensities for each molecular formula. The 95 percentile of the RSD values were used as threshold and any change in normalized peak intensity among different samples above this percent value is considered as statistical significant difference (**Figure S3**). ΔRI values corresponding to the RSD threshold were calculated (ΔRI < 0.43; ΔRI > 0.57). In the following, ΔRI values above 0.57 were considered to indicate that the respective compound is enriched in the sample, and ΔRI values below 0.43 indicates the respective compound is enriched in the reference.

Results and discussion

Permeability of the membrane

The selection of an appropriate dialysis membrane is essential for exposing nanoparticles to DOM under field conditions. In particular, the molecular weight cut-off (MWCO) should be high enough for the dissolved components of natural water to diffuse freely through the membrane, to simulate the river composition to a good extent inside the dialysis bag. On the other side, the membrane should not be permeable towards nanoparticles, in this study represented by n-TiO_2.

Figure 1 shows the HR-TEM image of pristine n-TiO_2 with diameters in the range of 20-50 nm. Hence, the average pore size of the applied dialysis bag should be significantly lower than 20 nm to retain the nanoparticles. Symmetrically, the natural colloids larger than the membrane pore size will not permeate through the membrane, thus simplifying the analytical procedure for the subsequent surface analysis of the DOM-coated nanoparticles.

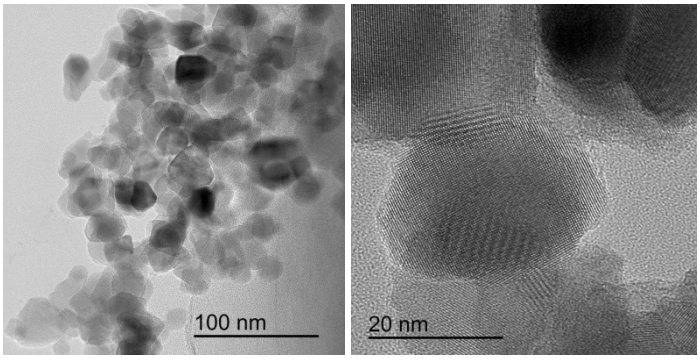

Figure 1: HR-TEM images of pristine n-TiO_2.

Table 2 shows the retention rate of n-TiO_2 depending on the MWCO (20, 100, 300 kDa) after two and seven days exposure. The initial Ti-content of river water was below the detection limit of the ICP-OES (**Table S2**). The retention rates were all higher than 90% . High retention values are expected considering the smallest size of n-TiO_2 (20-50 nm) compared to the pore size of the membranes (5-20 nm). Furthermore, n-TiO_2 nanoparticles were agglomerating in the river water due to the almost neutral pH (close to the isoelectric point of P25) [42] and the presence of different ions. [24] Therefore, the non-permeability of the membrane to nanoparticles can be improved when the nanoparticles are agglomerating in the natural water. Hence, the colloidal stability in natural water has to be considered in the choice of the membrane cut-off in addition to the size of primary particles.

Table 2: retention rate in % of n-TiO_2 inside the dialysis bags after 2 and 7 days incubation in river water

	Retention rate in %		
Days	20 kDa (~ 5nm)[1]	100 kDa (~ 10nm)[1]	300 kDa (~ 20nm)[1]

2	92.9 (± 3.6)[2]	93.8 (± 4.2)[2]	92.4 (± 5.3)[2]
7	92.8 (± 5.4)[2]	92.8 (± 3.1)[2]	90.6 (± 8.3)[2]

[1] There is no direct correlation between pore dimension (nm), and the molecular size cut-off (kDa); however, the manufacturer provides some approximations. [28]

[2] Standard deviation

Permeability of the membrane to dissolved organic matter (DOM) via free diffusion was evaluated using three-dimensional excitation-emission-matrix fluorescence spectroscopy (EEM). Four typical excitation/emission peaks have been observed in surface waters: [43] α (Ex/Em ~ 340/420), α′(Ex/Em ~ 250/430), β (as a shoulder on the α peak Ex/Em ~ 300/420), and ϒ (Ex/Em ~ 280/350). Among them, α , and α′ have been attributed to the carboxylic and phenolic groups, respectively, [16] β to weakly humified structures, simple phenols, coumarins and alkaloids, [44] and ϒ to proteins. [45] **Figure 2** depicts the EEM fluorescence map of the river water inside and outside of the dialysis bag (100 kDa) exposed to river water for 1 week. The similarity of the signals suggest that The DOM fluorophores are similar in terms of quantitiy and quality, therefore, the membrane is probably permeable to most part of DOM, including proteins (similar ϒ signals). These results suggest that a cut-off of 100 kDa is large enough for DOM in natural water to permeate. Since we kept the possibility to apply the present method to particles smaller than 20 nm but larger than 10 nm such as some n-TiO_2 found in sunscreens [5] and avoid the presence of small natural colloids with the DOM-coated n-TiO_2, 100 kDa was selected for further optimization.

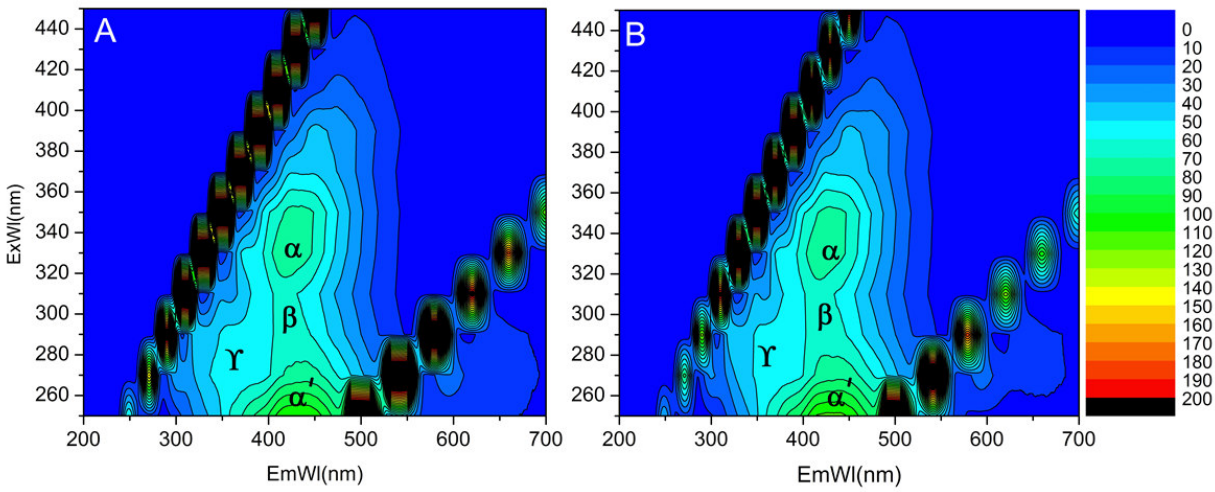

Figure 2: Fluorescence EEMs of A) inside and B) outside of the dialysis bag after one week of exposure to river water in the lab (the color scale depicts the intensity).

The exposure time of the dialysis bags to the river water is another important factor to optimize. On one hand, this time should be long enough to reach the equilibrium of DOM between inside and outside of the dialysis bags and to allow sufficient reaction time for nanoparticles; on the other hand, it should be short enough not to cause the decomposition of the membrane (chemical- and bio-degradation) in the river water. The optimal exposure time depends on the molecular cut-off and on the environmental conditions. **Figure 3** (left axis) shows the dissolved organic carbon (DOC) of the river sample (DOC around 6.5 ppm) inside and outside of a dialysis bags initially filled with distilled water over one week under laboratory conditions. The initial DOC inside the dialysis bag was zero. Over time, the DOC inside dialysis bag increased due to free diffusion of DOM from river water toward inside the dialysis bag. By three hours, the measured DOC inside and outside of the dialysis bag became similar and remained stable indicating that the system reached equilibrium in less than 3 h and up to 48 h. The difference between the DOC in the blank river water and with dialysis (about 13%) is probably due to organic leaching of the membrane and the closures. [46] This problem is not of relevance under field conditions since the volume of the water outside the bag is nearly infinite compared to the volume inside the membrane. Thus, the organic leaching cannot accumulate significantly near the bag.

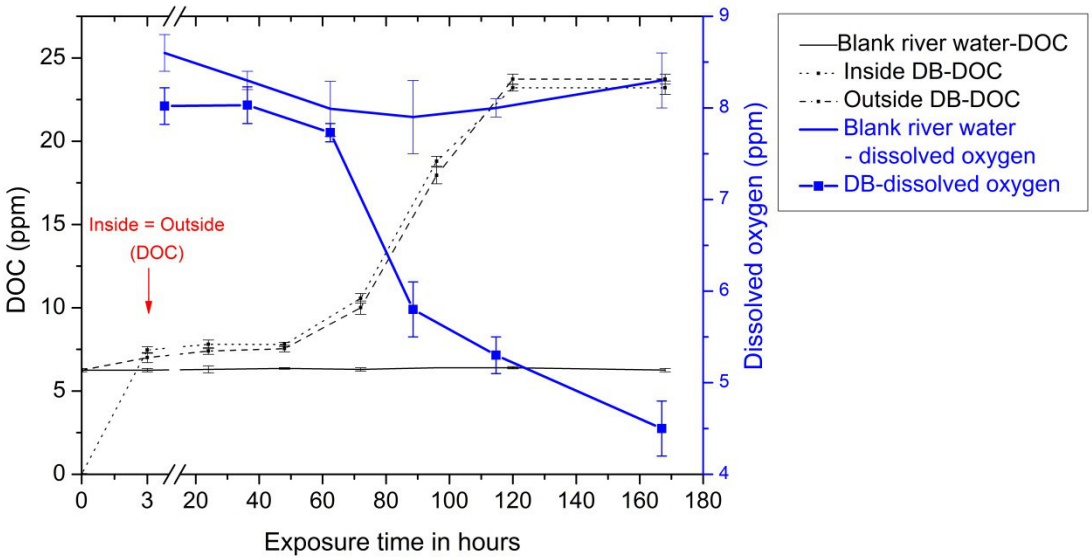

Figure 3: DOC (left axis), and dissolved oxygen (right axis) of the river water inside and outside dialysis bags (DB) initially filled with distilled water and immersed in river water at room temperature (Error bars depict standard deviation).

After 48h, there is a large increase in DOC concentration inside and outside the dialysis bag. This increase is most probably due to microbial activity leading to membrane decomposition [47] as suggested by the parallel decrease in dissolved oxygen (**Figure 3**, **right axis**). [48] Since the parallel increase in DOC, and decrease in dissolved oxygen were not observed in the blank river water, the dialysis bag is most probably the actual substrate for the microbial development under conditions causing the membrane to decompose over time. In order to overcome this drawback for studies requiring exposure times longer than 48h, we suggest modifying dialysis membranes to suppress microbial proliferation by using antibacterial agents in the membrane [47] or applying more robust membranes to microbial activity such as PVDF.

It has to be noted that, under different conditions (e.g. higher temperatures, high concentrations of nutrient, etc.), the decomposition of the membrane can be significantly faster. Therefore, we recommend keeping the exposure time as low as necessary for the equilibration of the DOC concentration inside the bag, while covering the relevant variations of environmental factors (e.g. day and night conditions) to be studied.

In addition to DOC and nanoparticles, the ability of inorganic ions to diffuse through the membrane was tested with river water under laboratory conditions after one week of exposure to river water. At room temperature, the pH remains stable inside and outside of the dialysis bag (pH = 7.2). However, the conductivity reduced about 55% inside the bag. This can be due the discrimination of some ions during the permeation or to bacterial growth. [49] To identify the source of this discrepancy we determined the total concentration of a selection of the most common elements in surface waters inside and outside the dialysis bag using ICP-OES. For most monitored elements, the equilibrium could be reached resulting in similar concentrations inside and outside the dialysis bags (**Figure 4**). Notable exceptions are Al, Fe, and Mn whose total concentrations inside the bag decreased more compared to other elements (30-60%). This is probably due to their high valencies when present as ions (Al: +3, Fe: +2 and +3, Mn: +2,+4, and +7), which increases the probability to interact with the cellulose ester membrane. [50] On the other hand, these elements have been often observed as particulate matter, colloidal or not, in surface waters, [51,52] which would drastically reduce their ability to diffuse through the membrane.

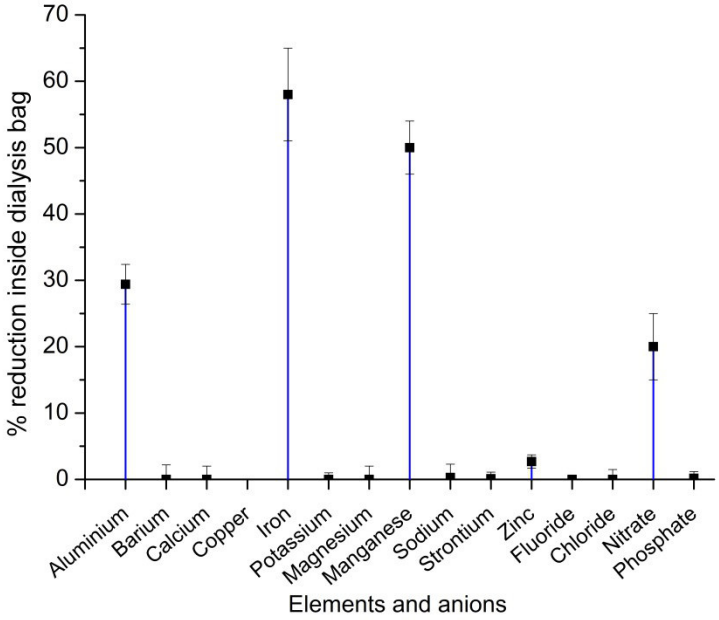

Figure 4: The percentage of reduction of elements and anions by passing through the dialysis bags (compared to outside). Error bars depict standard deviation.

A complete equilibrium was reached for anion concentrations, as observed for the elements, except for nitrate with 20 % reduction (**Figure 4**). The highest reduction observed for nitrate can be due to the nitrate reduction caused by the microbial activity on the substrate of the dialysis bag after one week of exposure to river water. [53] Therefore, the observed decrease in conductivity can be partly due to a lower amount of natural colloids carrying charges and to lower nitrate concentration related to microbial activity, whereas other factors involving microbial activity cannot be ruled out.

Membrane fouling

Membrane fouling occurs when biotic or abiotic materials obstruct pores, thus reducing the permeability of the membrane. Fouling in natural waters, with a complex mixture of particulate and dissolved components, is one of the important processes reducing the permeability of membranes by reducing the pore size of the membrane. [54] Since drying of the membrane reduces drastically the pore size of dialysis membranes, [55] we determined the pore size of the membranes used for DOM exposure using NMR relaxometry and AFM under wet conditions. [56,57] NMR relaxometry enables an in situ estimation of a pore size distribution averaged over the whole sample, while AFM enables imaging of the pore system at some selected spots at the surface of the membrane. Therefore, the combination of these two complementary methods is highly valuable for obtaining information of the pore size under wet conditions.

Pore size distribution measured by NMR relaxometry

To investigate the probable effect of water medium (e.g. cations) on spin-spin relaxation time (T_2), bulk water media (distilled water, and river water with and without n-TiO_2) were firstly measured (**Figure 5 - dash lines**). There was no significant difference (t-test, 95%) in terms of T_2 distribution modes among the bulk media; therefore, the T_2 of water-filled pores was independent of the medium itself.

Figure 5 (solid lines) depicts the T_2 measurements of water-filled pores of the dialysis bags in three different water media (distilled water, river water with and without n-TiO_2). In contrast to bulk water samples, the T_2 distributions of dialysis membrane samples depict two distinguished T_2 peaks representing the hierarchical structure in applied dialysis bags (cellulose ester). [30,58] Since the characteristic pore size of the membrane (r) and the T_2 of water-filled pores are proportional, [30] the larger T_2 (around 2000-3000 ms) indicates the slower relaxation and a larger pores, and smaller T_2 (200-300 ms) indicates faster relaxation and smaller pores. In addition, the larger T_2 distribution is the result of a mixed contribution between the water molecules absorbed on the surface of the membrane and free state; both states merge into one peak in the NMR relaxation spectra. [30]

Based on t-test, we did not observe any significant difference in the T_2 distributions of dialysis membranes in different water media (distilled water, river water with and without n-TiO_2). This suggests that, under the applied conditions, the overall pore size of the dialysis bags is not changing significantly. Therefore, the membrane fouling that causes changing the pore size is negligible.

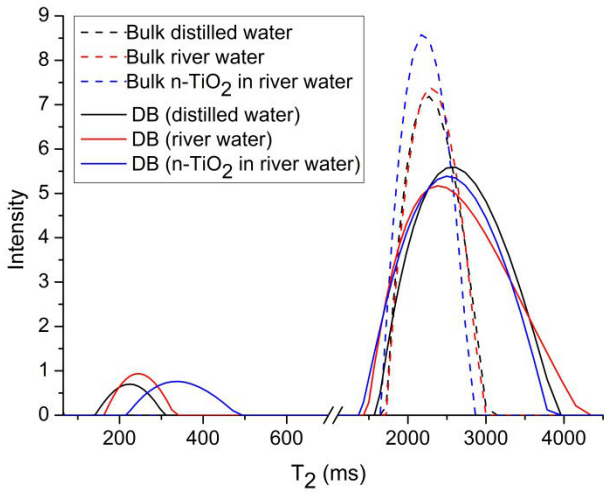

Figure 5: NMR relaxation spectra (T_2) of the ^1H spins of the bulk samples of distilled water, river water, and n-TiO_2 in river (dash line), and the water-filled pores of dialysis bags (DB) incubated in the corresponding water media for one week (solid line). Each sample was measured in triplicates and the T_2 distributions are averaged over the corresponding replicates.

In order to verify that pore clogging can actually be detected using NMR relaxometry, measurements were performed with membrane dried under ambient conditions. Since drying of dialysis membrane is known to induce an irreversible collapse of the pores, [28] we expected the pore size to be drastically reduced after drying. Since the presence of water molecules in the pores is required for characterizing the pore size using NMR relaxometry, the dried membrane was rewetted for 24 hours prior to T_2 measurement. The first peak of the T_2 distribution corresponding to small pores of dried dialysis membranes after rewetting (**Figure 6-clogged pores**) was significantly smaller (t-test, 95%) compared to non-dried membranes (**Figure 6-open pores**). Considering a T_2 value for small pores around 70 ms as an extreme case for collapsed of the membrane structure, it can be concluded that all dialysis membrane samples in water media (**Figure 4-solid line**) with T_2 values of 200-300 ms did not experience extended fouling, which would have led to a significant reduction of pore size.

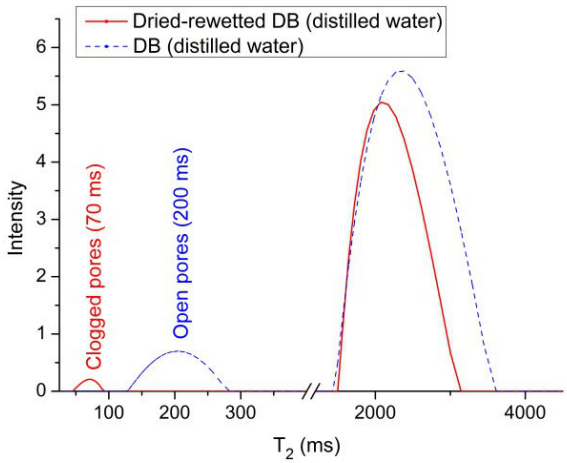

Figure 6: T_2 distribution comparison of dried-rewetted dialysis bags (clogged pores) and wet dialysis bag (open pores) in distilled water.

Pore size distribution measured by AFM

Figure 7 shows the AFM height and phase images of a dialysis membrane measured in distilled water. All the measurements were carried out in the fluid mode for avoiding drying of the sample. Furthermore, this mode enables using the same media as during the permeability experiments (river water with and without n-TiO_2), thus providing a more realistic assessment of the membrane pore size.

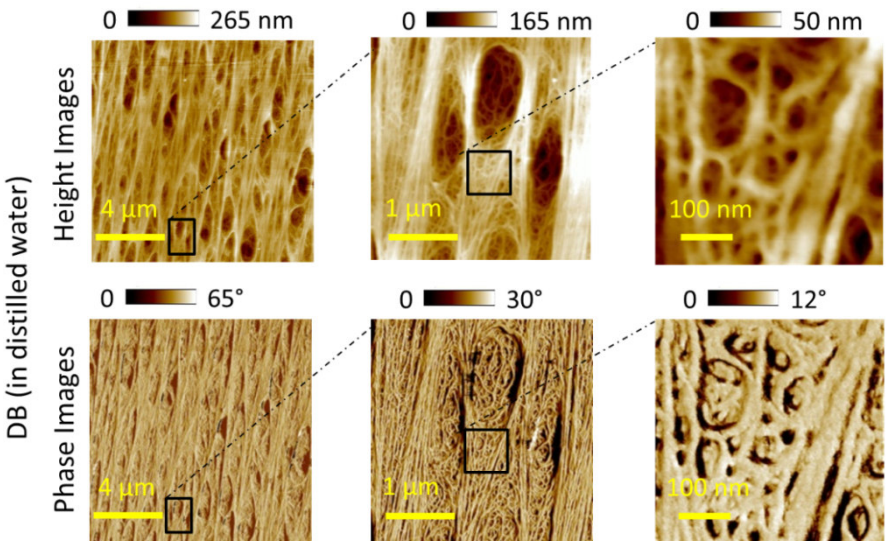

Figure 7: AFM height (top) and phase (bottom) images of the dialysis bag (DB) in distilled water measured in fluid mode.

The images exhibit the hierarchical porous structure of the dialysis bag. Three different areas are distinguishable in the images ranging from the nanometer to the micrometer scale: 1) a microporous structure with a polydisperse size distribution, 2) at higher magnification, a nanoporous network covering the whole sample including inside the micropores, and 3) a lamellar substructure. AFM images of dialysis bags in the river water (with and without n-TiO_2) depict an overall lower resolution compared to the samples measured in distilled water (**Figures S4-S5**) probably due to ionic screening charges in river water (Bruker.com).

The pore size distribution of dialysis bags in different media (**Figure 8**) shows a hydrodynamic diameter mode of 4 nm for all the samples. Besides, the observed differences between the pore sizes of the dialysis bags in different water media were not significant; in agreement with the results of NMR relaxometry. The determination of the average pore diameter of a three-dimensional porous structure based on two-dimensional images can only be an approximation based on several assumptions. Therefore, the absolute values of the pore size reported here should be taken as a first estimation and used for comparison purposes only.

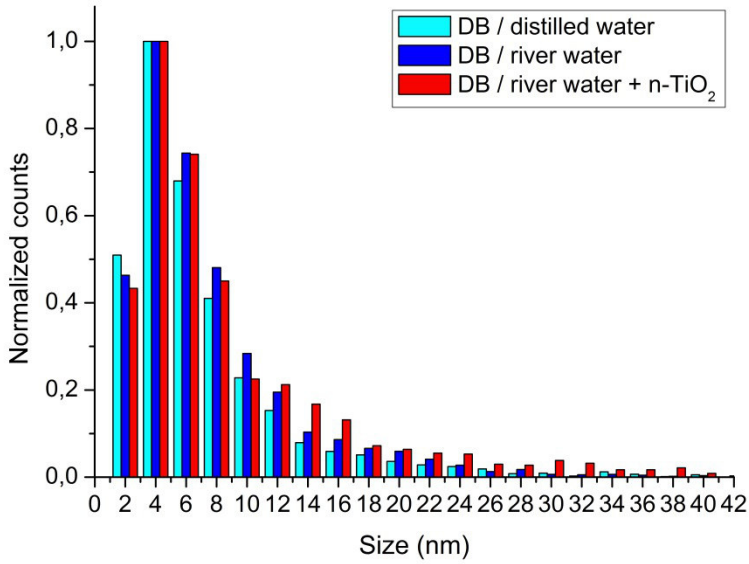

Figure 8: Pore size distribution of dialysis bags (DB) in different water media determined using AFM in fluid mode (Six AFM regions of interest were used for each sample).

Field experiment

Based on the previous method development, cylindrical cellulose ester dialysis bags with MWCO of 100 kDa were chosen to carry out a proof of concept of investigating the interaction of n-TiO_2 with natural DOM under natural conditions. After one week of exposure in the river, the samples (inside the dialysis bag) were collected in polypropylene centrifuge tubes and transported immediately to the nearly located laboratory. The n-TiO_2 were then separated using centrifugation for characterizing the sorption of NOM onto n-TiO_2. In general, the composition and quantity of DOM in natural waters vary over time[59] and investigations on the sorption require monitoring these variations over the deployment period. However, the concentrations inside and outside the dialysis bag equilibrate in less than a few hours and the water composition was fairly stable over the time of this study (**table S1**). Hence, we assume that the compositions of water sampled outside and inside the dialysis bag are similar. To provide a reference for NOM (outside the dialysis bag), the river water was also collected in polypropylene centrifuge tubes on the last day of exposure.

Permeability of the membrane under field experiment: Fluorescence EEMs

Figure 9 shows the Fluorescence EEMs of the river water (A), and the river water diffused into the dialysis bag (B). In both samples, the EEM plots show four spectral features of the natural waters relate to α, α′, β, and ϒ corresponding respectively to carboxylic, phenolic, alkaloids, and protein groups (see discussion above).

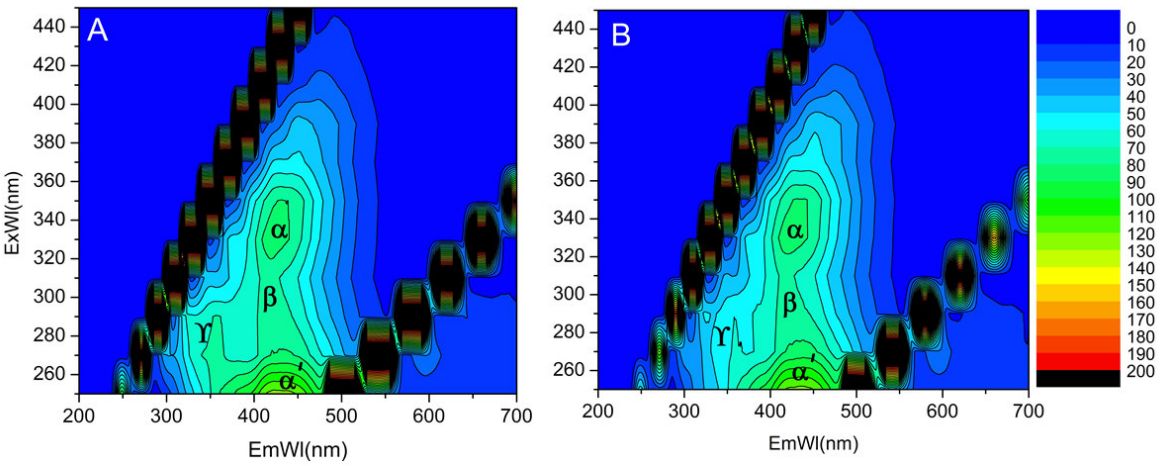

Figure 9: Fluorescence EEMs of the samples carried out in the field A) river water B) river water inside the dialysis bag (the color scale depicts the intensity a.u).

As it can be seen, α, α´, and β peaks of the river water are similar in inside and outside of the DB. It can suggest that the composition of DOM of the river water inside the DB is similar to the natural water to a good extent.

Figure 6S depicts the Fluorescence EEM of the supernatant of the river water inside DB in presence of n-TiO_2. All the mentioned peaks in the river water (α, α´, β, and ϒ) are present with reduced intensities in this sample. An indirect effect of the sorption of DOM onto n-TiO_2 could explain these differences. However, one should notice that the quantitative interpretation of fluorescence results for such complex mixtures is far from trivial and should be considered as a first approach in the frame of this proof of concept. Hence, the Fluorescence EEMs results can be investigated qualitatively not quantitatively. However, the results show the DOM permeates the membrane under field condition and the made observations are similar to the ones made in the lab. The biological activities induced by the membrane decomposition seem not to impair sensibly the permeability of the membrane and may, therefore, be of little importance under field conditions.

Since the results of fluorescence spectroscopy are just expressing the fluorophore groups in the river water, and the activity of lipids or polysaccharides, for instance, cannot be monitored, the water media were further investigated with FT-ICR-MS.

Permeability of the membrane under field experiment: FT-ICR-MS

Ultrahigh resolution Fourier-transform ion cyclotron resonance mass spectrometry (FT-ICR-MS) was used to gain detailed insight in the molecular composition of river water DOM inside and outside the dialysis bag.

3766 (58%) out of 6468 formulas were shared between all three river samples (outside the dialysis bag, and inside the dialysis bag with and without n-TiO_2), while 1181 (18%) and 1539 (24%) formulas occurred only in

one and two samples, respectively (**Figure S7**). As expected for terrestrial derived DOM, there was a large dominance of CHO (53%) compounds over CHNO (35%) and CHOS (10%) (**Table S4**).

Some compounds were depleted (ΔRI < 0.43) in the water outside vs inside the bag (n = 554) but show a homogenous distribution in the van Krevelen (vK) space as expected for analytical noise **(Figure 10**). However, based on intensity differences between river water inside the dialysis bags and river water outside the bag, there emerges a clear pattern for compounds enriched inside the bag (ΔRI > 0.57, n = 591). They represent compounds which are highly aliphatic (H/C = 1.622 ± 0.178), and cover a broad range of oxygenation (O/C = 0.403 ± 0.108).

Cellulose acetate is biodegradable in presence of esterases which is produced by different classes of microorganisms. [60] Upon biodegradation, cellulose acetate bears deacetylation and breaking down cellulose backbone [61] into smaller chains or glucose monomers, which are potential sources of energy for further microbial activities. Hence, the observed pattern of enriched compounds inside the dialysis bag (compared to the river water) may point to microbial induced degradation of the membrane. This is in agreement with the results of DOC and dissolved O_2 (**Figure 3**) showing respiration within and DOC leaching from the bag in one week under laboratory conditions.

Interestingly, compounds with similar chemical properties (H/C = 1.539 ± 0.368, O/C = 0.401 ± 0.148) were depleted when n-TiO_2 was added to the bags compared to the bags without n-TiO_2 (**Figure S8**) i.e. the enrichment observed in the river water inside the dialysis bag is not observed with n-TiO_2 present. While the enriched compounds inside the bag are mostly CHO (73%), the depleted compounds with n-TiO_2 contain a larger fraction of CHNO formulas (47%). In the field experiment, under the assumption of thermodynamic equilibrium, any preferential sorption of DOM on the n-TiO_2 can be compensated by river water from outside the dialysis bag. This assumption is acceptable considering the relatively short equilibration time measured in the laboratory experiments (less than 3 h, **Figure 3**) and the stability of the river water chemical parameters over months (**Table S1**). Therefore, the observed differences in DOM composition are probably not related only to sorption, but to the effect of n-TiO_2 on biodegradation of the membrane. Indeed, Lazic et al. reported the negative influence of n-TiO_2 on biodegradation of cellulose. [62]

In order to explore this hypothesis, we determined the measured DOC and dissolved oxygen (DO) of the river water inside the dialysis bag with and without n-TiO_2 over a week under laboratory conditions (**Figure S9).** In both cases, DOC was increasing over a week; however, less increase was observed in presence of n-TiO_2. Since the control samples of the river water with and without n-TiO_2 showed a similar DOC, sorption cannot be the determinant factor of the decreased DOC production inside the bag in presence of nanoparticles. Furthermore,

DOC increasing occurred parallel to DO decreasing (**Figure S9**) with less reduction observed inside the dialysis bag in presence of n-TiO_2 while the control samples of the river water with and without n-TiO_2 showed almost the same DO. Therefore, we conclude that n-TiO_2 reduces the biodegradation of cellulose ester under laboratory and field conditions.

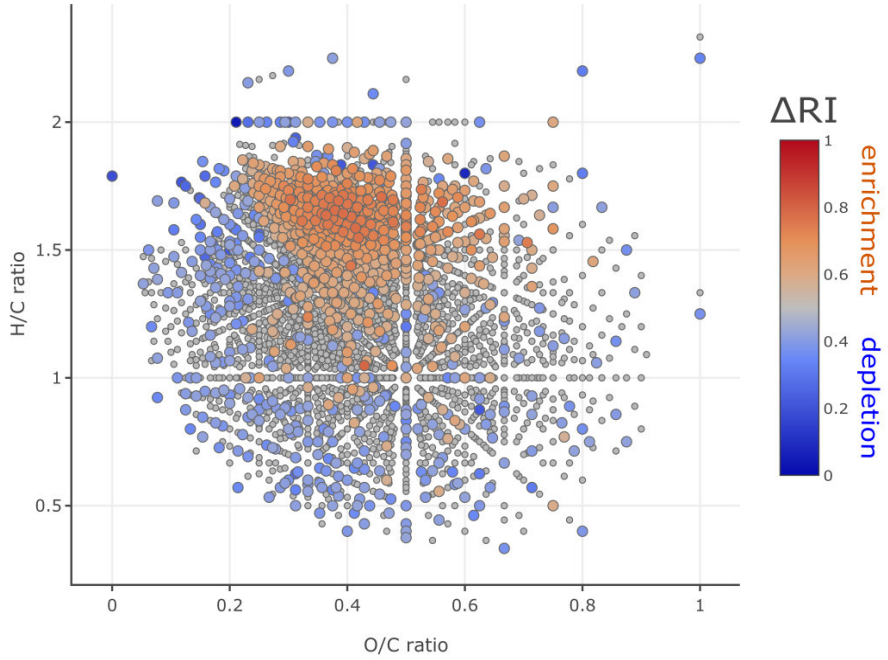

Figure 10: Van Krevelen diagram with intensity differences for river water inside the dialysis bags vs river water. ΔRI values above 0.57 (red) were considered to indicate that the respective compound is enriched inside the dialysis bags, and ΔRI values below 0.43 (blue) indicates the respective compound is depleted inside the dialysis bag.

Sorption of DOM onto n-TiO_2: ATR-FTIR

The ATR-FTIR spectra of n-TiO_2, and n-TiO_2 exposed to the river water are shown in **Figure 11**. There are two bands in both samples, the peak around 1640 cm^{-1} is attributed to the bending vibration of the O-H bond of chemisorbed water and the broad peak around 3350 cm^{-1} corresponds to the surface adsorbed water and hydroxyl groups. A prominent band occurring at 430cm^{-1} due to Ti-O, and Ti-O-Ti stretching vibration modes is shifted to lower frequency after exposing to river water; [63] probably due to the interaction of Ti-O with the DOM of the river water. The major functional groups in aquatic humic substances are carboxylic acid, hydroxyl, phenolic, and carbonyl groups (1100-1700 cm^{-1}), [26] which were seen in the river water sample (**Figure S10**). After

exposing n-TiO_2 to the river water, the band at 1400 cm^{-1} (**Figure 11**) can be attributed to carboxylic acid groups of the river water sorbed onto nanoparticles. The C-H stretching vibrations (CH_2) between 2950-2850 clearly indicate organic matter on the river exposed sample. In addition, the agglomeration of the nanoparticles in the river media could cause the observed band broadening. [64]

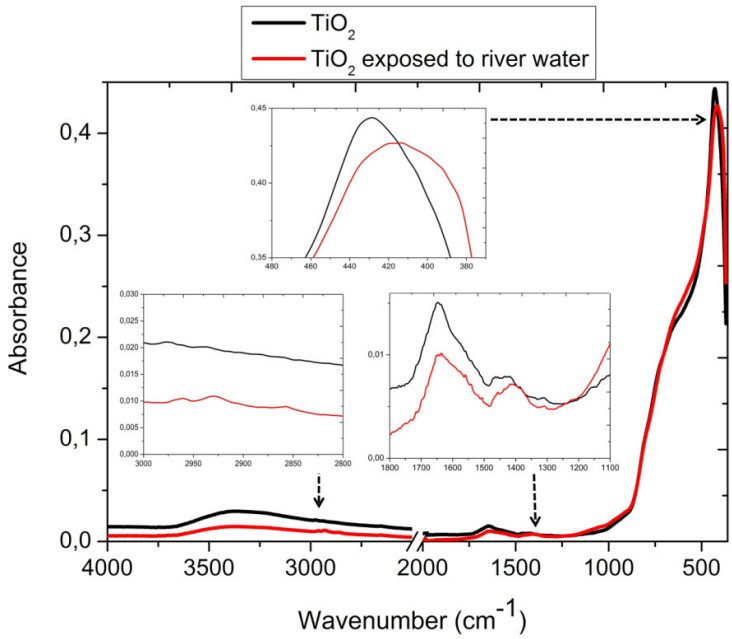

Figure 11: ATR-FTIR spectra of n-TiO_2, and n-TiO_2 exposed to river water in field experiment.

Sorption of DOM onto n-TiO_2: CHNS

Elemental analysis in **Table 3** depicts that the carbon, nitrogen, hydrogen, and sulfur content of river water (freeze-dried), n-TiO_2, and n-TiO_2 exposed to river water. The CHNS-contents in n-TiO_2 exposed to River water were higher than in pristine n-TiO_2 probably indicating the sorption of DOM onto n-TiO_2. **Figure 12** depicts the Euclidean distances allows comparing the elemental composition of the three treatments where "A" is assigned to n-TiO_2, "B" to river water, and "C" to n-TiO_2 exposed to river water (A-B: 0.495 ± 0.25, A-C: 0.528 ± 0.24, B-C: 0.0965 ± 0.18). Since the point corresponding to n-TiO_2 exposed to river water is closer to the river water than to the pristine n-TiO_2 (**Figure 12**: B-C < A-C), we conclude that the organic matter adsorbed onto the nanoparticles under field condition does not experience strong fractionation. This results in an NOM-coating chemically close to river water DOM. Furthermore, comparing the absolute absorbance values of the elements depicted that although there is a high difference between the amount of river water in two samples of "B" and "C" (250 ml of freeze-died river water in "B" compared to few µL of residual river water on n-TiO_2 in "C"), the absorbance is comparable. Hence, contribution of the residual river water to the CHNS-signal of the nanoparticles in river water is negligible. Combining the hints provided by EEM fluorescence, ATR-FTIR, and

CHNS analyses, we can conclude that the sorption of DOM occurred under field condition and that the proposed concept is valid.

Table 3 Elemental content (CHNS) in river water, n-TiO_2, and n-TiO_2 exposed to River water

Element content (wt %)	n-TiO_2	n-TiO_2 exposed to River water	River water
C	0.012	1.23	6.15
H	0.057	0.18	1.53
N	0.107	0.26	1.29
S	0.13	0.74	4.84

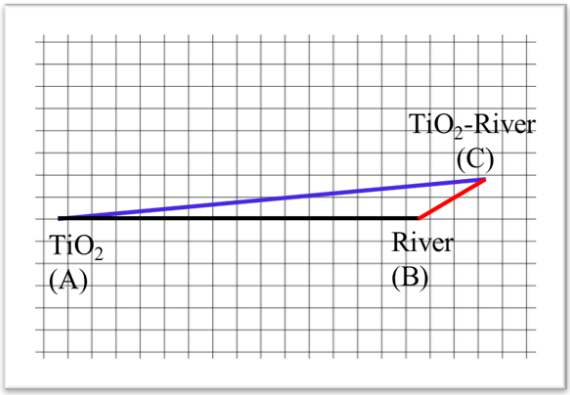

Figure 12: Euclidean distances calculated from the normalized C-, H-, N-, and S-contents (four dimensional space) of River water, n-TiO_2, and n-TiO_2 exposed to River water where A-B: 0.495±0.25, A-C: 0.528 ± 0.24, B-C: 0.0965±0.18.

Conclusion

In this work, we introduced dialysis membrane as a passive reactor to produce nanoparticles with natural coating. Such particles could be useful to study the fate and toxicity of nanoparticles under natural conditions. Since nanoparticles from 20 nm are successfully retained in the reactor and most of the DOM can permeate through the membrane and reach the nanoparticle surface, we conclude that the concept is valid. Furthermore, the sorption of DOM onto n-TiO_2 was evaluated by ATR-FTIR and CHNS elemental analysis of the nanoparticles before and after exposure to the river water which both depicted the occurrence of sorption under applied conditions. Further validation will include testing the performance of the reactor under various conditions and in differing surface waters. For exposure times longer than two days, the microbial activity due to the degradation of the membrane may interfere with the sorption processes. Optimizing the membrane properties

and sample preparation in order to minimize this effect can help in this respect. Finally, for future studies, more advanced analytical methods are required to characterize NOM-engineered nanoparticles corona.

Acknowledgments

This research was funded by the German Research Foundation, research unit INTERNANO (FOR1536 "Mobility, aging and functioning of engineered inorganic nanoparticles at the aquatic–terrestrial interface", subprojects SCHA849/16). The authors would like to thank Wolfgang Fey, Karin Meyer, and Doris Burgard for ICP-OES, DOC, and CHNS measurements, respectively. The authors also acknowledge Jan Kaesler for FT-ICR MS measurements and are grateful for using the analytical facilities of the Centre for Chemical Microscopy (ProVIS) at the Helmholtz Centre for Environmental Research, Leipzig which is supported by the European Regional Development Funds (EFRE - Europe funds Saxony) and the Helmholtz Association.

References

1 N. C. Birben, C. S. Uyguner-Demirel, S. S. Kavurmaci, Y. Y. Gürkan, N. Turkten, Z. Cinar and M. Bekbolet, Application of Fe-doped TiO2 specimens for the solar photocatalytic degradation of humic acid, *Catalysis Today*, 2017, **281**, 78–84.

2 F. Loosli, P. Le Coustumer and S. Stoll, Effect of electrolyte valency, alginate concentration and pH on engineered TiO2 nanoparticle stability in aqueous solution, *Science of the Total Environment*, 2015, **535**, 28–34.

3 V. Adam, S. Loyaux-Lawniczak and G. Quaranta, Characterization of engineered TiO2 nanomaterials in a life cycle and risk assessments perspective, *Environmental Science and Pollution Research*, 2015, **22**, 11175–11192.

4 Y. S. Sahu, Nano Titanium Dioxide Market by Application (Paints & Coatings, Pigments, Cosmetics, Plastics, Energy and others) - Global Opportunity Analysis and Industry Forecast, 2014 - 2022, *Allied Market Research*, 2016, 119.

5 A. Philippe, J. Košík, A. Welle, J.-M. Guigner, O. Clemens and G. E. Schaumann, Extraction and characterization methods for titanium dioxide nanoparticles from commercialized sunscreens, *Environmental Science: Nano*, 2018, **5**, 191–202.

6 A. P. Gondikas, F. von der Kammer, R. B. Reed, S. Wagner, J. F. Ranville and T. Hofmann, Release of TiO2 nanoparticles from sunscreens into surface waters: a one-year survey at the old Danube recreational Lake, *Environmental science & technology*, 2014, **48**, 5415–5422.

7 M. Bundschuh, J. Filser, S. Lüderwald, M. S. McKee, G. Metreveli, G. E. Schaumann, R. Schulz and S. Wagner, Nanoparticles in the environment: where do we come from, where do we go to?, *Environmental Sciences Europe*, 2018, **30**, 6.

8 G. E. Schaumann, A. Philippe, M. Bundschuh, G. Metreveli, S. Klitzke, D. Rakcheev, A. Grün, S. K. Kumahor, M. Kühn, T. Baumann and others, Understanding the fate and

biological effects of Ag-and TiO2-nanoparticles in the environment: the quest for advanced analytics and interdisciplinary concepts, *Science of the Total Environment*, 2015, **535**, 3–19.

9 A. Philippe and G. E. Schaumann, Interactions of dissolved organic matter with natural and engineered inorganic colloids: a review, *Environmental science \& technology*, 2014, **48**, 8946–8962.

10 C. Zhang, J. Lohwacharin and S. Takizawa, Properties of residual titanium dioxide nanoparticles after extended periods of mixing and settling in synthetic and natural waters, *Scientific Reports*, 2017, **7**, 9943.

11 S. Valencia, J. M. Marín, G. Restrepo and F. H. Frimmel, Evaluation of natural organic matter changes from Lake Hohloh by three-dimensional excitation-emission matrix fluorescence spectroscopy during TiO2/UV process, *Water research*, 2014, **51**, 124–133.

12 N. Sani-Kast, J. Labille, P. Ollivier, D. Slomberg, K. Hungerbühler and M. Scheringer, A network perspective reveals decreasing material diversity in studies on nanoparticle interactions with dissolved organic matter, *Proceedings of the National Academy of Sciences*, 2017, 201608106.

13 C. Nickel, B. Hellack, A. Nogowski, F. Babick, M. Stintz, H. Maes, A. Schäffer and T. Kuhlbusch, Mobility, fate and behavior of TiO2 nanomaterials in different environmental media, *Environmental Research of the Federal Ministry for the Environment*.

14 M. Luo, Y. Huang, M. Zhu, Y. Tang, T. Ren, J. Ren, H. Wang and F. Li, Properties of different natural organic matter influence the adsorption and aggregation behavior of TiO2 nanoparticles, *Journal of Saudi Chemical Society*.

15 M. Drosos, M. Ren and F. H. Frimmel, The effect of NOM to TiO2: interactions and photocatalytic behavior, *Applied Catalysis B: Environmental*, 2015, **165**, 328–334.

16 W. Chen, C. Qian, X.-Y. Liu and H.-Q. Yu, Two-dimensional correlation spectroscopic analysis on the interaction between humic acids and TiO2 nanoparticles, *Environmental science & technology*, 2014, **48**, 11119–11126.

17 S. Shakiba, A. Hakimian, L. R. Barco and S. M. Louie, Dynamic Intermolecular Interactions Control Adsorption from Mixtures of Natural Organic Matter and Protein onto Titanium Dioxide Nanoparticles, *Environmental science & technology*, 2018, **52**, 14158–14168.

18 J. Namieśnik, B. Zabiegała, A. Kot-Wasik, M. Partyka and A. Wasik, Passive sampling and/or extraction techniques in environmental analysis: a review., *Anal Bioanal Chem*, 2005, **381**, 279–301.

19 A. Kot, B. Zabiegala and J. Namiesnik, Passive sampling for long-term monitoring of organic pollutants in water, *TrAC Trends in Analytical Chemistry*, 2000, **19**, 446–459.

20 T. Górecki and J. Namie'snik, Passive sampling, *TrAC Trends in Analytical Chemistry*, 2002, **21**, 276–291.

21 D. A. Vroblesky, J. Manish, J. Morrell and J. Peterson, Evaluation of passive diffusion bag samplers, dialysis samplers, and nylon-screen samplers in selected wells at Andersen Air Force Base, Guam, March-April 2002, *US Geological Survey Water-Resources Investigations Report*, 2003, 03–4157.

22 B. E. Vencalek, S. N. Laughton, E. Spielman-Sun, S. M. Rodrigues, J. M. Unrine, G. V. Lowry and K. B. Gregory, In situ measurement of CuO and Cu (OH) 2 nanoparticle dissolution rates in quiescent freshwater mesocosms, *Environmental Science \& Technology Letters*, 2016, **3**, 375–380.

23 P. Benes and E. Steinnes, In situ dialysis for the determination of the state of trace elements in natural waters, *Water Research*, 1974, **8**, 947–953.

24 P. Wang, Aggregation of TiO2 Nanoparticles in Aqueous Media: Effects of pH, Ferric Ion and Humic Acid, *Int. J. Environ. Sci. Nat. Res*, 2017, **1**, 555575.

25 W. Wu, G. Shan, Q. Xiang, Y. Zhang, S. Yi and L. Zhu, Effects of humic acids with different polarities on the photocatalytic activity of nano-TiO2 at environment relevant concentration, *Water research*, 2017, **122**, 78–85.

26 K. J. Howe, K. P. Ishida and M. M. Clark, Use of ATR/FTIR spectrometry to study fouling of microfiltration membranes by natural waters, *Desalination*, 2002, **147**, 251–255.

27 S. Jeon, S. Rajabzadeh, R. Okamura, T. Ishigami, S. Hasegawa, N. Kato and H. Matsuyama, The effect of membrane material and surface pore size on the fouling properties of submerged membranes, *Water*, 2016, **8**, 602.

28 https://www.repligen.com/dialysis-tubing-membranes.

29 M. Meyer, C. Buchmann and G. Schaumann, Determination of quantitative pore-size distribution of soils with 1H NMR relaxometry, *European journal of soil science*, 2018, **69**, 393–406.

30 C. Zhang, P. Li, Y. Zhang, F. Lu, W. Li, H. Kang, J. Xiang, Y. Huang and R. Liu, Hierarchical porous structures in cellulose: NMR relaxometry approach, *Polymer*, 2016, **98**, 237–243.

31 J. V. Bayer, F. Jaeger and G. E. Schaumann, Proton nuclear magnetic resonance (NMR) relaxometry in soil science applications, *The Open Magnetic Resonance Journal*, 2010, **3**, 15–26.

32 http://www.nanophys.kth.se/nanophys/facilities/nfl/afm/fast-scan/bruker-help/Content/Probe%20and%20Sample%20Guide/Samples/FS%20Fluid%20Sample %20Mounting.htm.

33 http://www.nanophys.kth.se/nanophys/facilities/nfl/afm/fast-scan/bruker help/Content/Fluid%20Imaging/FS%20Fluid%20Operation_Droplet.htm.

34 R. J. Peters, G. van Bemmel, N. B. Milani, G. C. den Hertog, A. K. Undas, M. van der Lee and H. Bouwmeester, Detection of nanoparticles in Dutch surface waters, *Science of the Total Environment*, 2018, **621**, 210–218.

35 J. Raeke, O. J. Lechtenfeld, M. Wagner, P. Herzsprung and T. Reemtsma, Selectivity of solid phase extraction of freshwater dissolved organic matter and its effect on ultrahigh resolution mass spectra, *Environmental Science: Processes & Impacts*, 2016, **18**, 918–927.

36 O. J. Lechtenfeld, G. Kattner, R. Flerus, S. L. McCallister, P. Schmitt-Kopplin and B. P. Koch, Molecular transformation and degradation of refractory dissolved organic matter in the Atlantic and Southern Ocean, *Geochimica et Cosmochimica Acta*, 2014, **126**, 321–337.

37 B. Koch, G. Kattner, M. Witt and U. Passow, Molecular insights into the microbial formation of marine dissolved organic matter: recalcitrant or labile?, *Biogeosciences*, 2014, **11**, 4173–4190.

38 P. Herzsprung, N. Hertkorn, W. von Tümpling, M. Harir, K. Friese and P. Schmitt-Kopplin, Understanding molecular formula assignment of Fourier transform ion cyclotron resonance mass spectrometry data of natural organic matter from a chemical point of view, *Analytical and bioanalytical chemistry*, 2014, **406**, 7977–7987.

39 P. Herzsprung, N. Hertkorn, W. von Tümpling, M. Harir, K. Friese and P. Schmitt-Kopplin, Molecular formula assignment for dissolved organic matter (DOM) using high-field FT-ICR-MS: chemical perspective and validation of sulphur-rich organic components (CHOS) in pit lake samples, *Analytical and bioanalytical chemistry*, 2016, **408**, 2461–2469.

40 T. Kind and O. Fiehn, Seven Golden Rules for heuristic filtering of molecular formulas obtained by accurate mass spectrometry, *BMC bioinformatics*, 2007, **8**, 105.

41 J. Raeke, O. J. Lechtenfeld, J. Tittel, M. R. Oosterwoud, K. Bornmann and T. Reemtsma, Linking the mobilization of dissolved organic matter in catchments and its removal in drinking water treatment to its molecular characteristics, *Water research*, 2017, **113**, 149–159.

42 M. Kosmulski, Isoelectric points and points of zero charge of metal (hydr) oxides: 50 years after Parks' review, *Advances in colloid and interface science*, 2016, **238**, 1–61.

43 B. Matthews, A. Jones, N. Theodorou and A. Tudhope, Excitation-emission-matrix fluorescence spectroscopy applied to humic acid bands in coral reefs, *Marine Chemistry*, 1996, **55**, 317–332.

44 P. Boguta and Z. Sokołowska, Interactions of Zn (II) ions with humic acids isolated from various type of soils. Effect of pH, Zn concentrations and humic acids chemical properties, *PLoS One*, 2016, **11**, e0153626.

45 M. Sierra, M. Giovanela, E. Parlanti and E. Soriano-Sierra, Fluorescence fingerprint of fulvic and humic acids from varied origins as viewed by single-scan and excitation/emission matrix techniques, *Chemosphere*, 2005, **58**, 715–733.

46 E. Khan and S. Subramania-Pillai, Effect of leaching from filters on laboratory analyses of collective organic constituents, *Proceedings of the Water Environment Federation*, 2006, **2006**, 901–918.

47 A. F. de Faria, A. C. M. de Moraes, P. F. Andrade, D. S. da Silva, M. do Carmo Gonçalves and O. L. Alves, Cellulose acetate membrane embedded with graphene oxide-silver

nanocomposites and its ability to suppress microbial proliferation, *Cellulose*, 2017, **24**, 781–796.

48 http://www.epa.gov/glindicators/water/oxygenb.html, Dissolved Oxygen Depletion in Lake Erie. In Great Lakes Monitoring.

49 K. Krishnamurti and S. Kate, Changes in electrical conductivity during bacterial growth, *Nature*, 1951, **168**, 170.

50 K. Andarany, A. Sagir, A. Ahmad, S. Deni and W. Gunawan, in *IOP Conference Series: Materials Science and Engineering*, 2017, vol. 237, p. 012042.

51 B. M. Tebo, J. R. Bargar, B. G. Clement, G. J. Dick, K. J. Murray, D. Parker, R. Verity and S. M. Webb, Biogenic manganese oxides: properties and mechanisms of formation, *Annu. Rev. Earth Planet. Sci.*, 2004, **32**, 287–328.

52 T. Rennert, Wet-chemical extractions to characterise pedogenic Al and Fe species-a critical review, *Soil Research*, 2019, **57**, 1–16.

53 M. Tiso and A. N. Schechter, Nitrate reduction to nitrite, nitric oxide and ammonia by gut bacteria under physiological conditions, *PloS one*, 2015, **10**, e0119712.

54 E. Fridjonsson, S. Vogt, J. S. Vrouwenvelder and M. Johns, Early non-destructive biofouling detection in spiral wound RO membranes using a mobile earth′ s field NMR, *Journal of Membrane Science*, 2015, **489**, 227–236.

55 Y. Qing, R. Sabo, Y. Wu, J. Zhu and Z. Cai, Self-assembled optically transparent cellulose nanofibril films: effect of nanofibril morphology and drying procedure, *Cellulose*, 2015, **22**, 1091–1102.

56 M. Hayama, K. Yamamoto, F. Kohori and K. Sakai, How polysulfone dialysis membranes containing polyvinylpyrrolidone achieve excellent biocompatibility?, *Journal of membrane science*, 2004, **234**, 41–49.

57 L. A. Neves, P. J. Sebastiao, I. M. Coelhoso and J. G. Crespo, Proton NMR relaxometry study of nafion membranes modified with ionic liquid cations, *The Journal of Physical Chemistry B*, 2011, **115**, 8713–8723.

58 S. Polarz, B. Smarsly and J. H. Schattka, Hierachical porous carbon structures from cellulose acetate fibers, *Chemistry of materials*, 2002, **14**, 2940–2945.

59 H. Van de Weerd, W. Van Riemsdijk and A. Leijnse, Modeling the dynamic adsorption/desorption of a NOM mixture: Effects of physical and chemical heterogeneity, *Environmental science \& technology*, 1999, **33**, 1675–1681.

60 K. Sayali, P. Sadichha and S. Surekha, Microbial esterases: an overview, *International Journal of Current Microbiology and Applied Sciences*, 2013, **2**, 135–146.

61 J. Puls, S. A. Wilson and D. Hölter, Degradation of Cellulose Acetate-Based Materials: A Review, *Journal of Polymers and the Environment*, 2011, **19**, 152–165.

62 V. Lazic, M. Radoicic, Z. Saponjic, T. Radetic, V. Vodnik, S. Nikolic, S. Dimitrijevic and M. Radetic, Negative influence of Ag and TiO2 nanoparticles on biodegradation of cotton fabrics, *Cellulose*, 2015, **22**, 1365–1378.

63 L. Saravanan, R. M. Kumar, A. Pandurangan and R. Jayavel, Synthesis and photophysical studies of PVP capped Titania Nanostrips for photocatalytic applications, *Optoelectronics and advanced materials-rapid comunications*, 2010, **4**, 1676–1680.

64 K. S. Babu, A. R. Reddy, C. Sujatha, K. V. Reddy and A. Mallika, Synthesis and optical characterization of porous ZnO, *Journal of Advanced Ceramics*, 2013, **2**, 260–265.